DFT screening of adsorption of biodiesel molecules on aluminum and stainless steel surfaces

Claudia Cantarelli, Benoît Darenne, Maira Alves Fortunato, Theodorus de Bruin, Dominique Costa

Results in Surfaces and Interfaces 6 (2022) 100050

Contents lists available at ScienceDirect

Results in Surfaces and Interfaces

journal homepage: www.elsevier.com/locate/rsurfi

DFT screening of adsorption of biodiesel molecules on aluminum and stainless steel surfaces

Claudia Cantarelli [a], Benoît Darenne [a], Maira Alves Fortunato [a], Theodorus de Bruin [a,*], Dominique Costa [b,*]

[a] IFP Energies nouvelles, Institut Carnot IFPEN Transports Energie, 1 et 4 avenue de Bois-Préau, 92852 Rueil-Malmaison, France
[b] PSL University, CNRS—Chimie ParisTech, Institut de Recherche de Chimie Paris/Physical Chemistry of Surfaces Group, 75005 Paris, France

ARTICLE INFO

Keywords:
α-Al_2O_3
α-Cr_2O_3
Adsorption
DFT-D
Hydroxylated surface

ABSTRACT

We present a Density Functional Theory (DFT) study of the adsorption of small organic molecules, taken as models of biodiesel autoxidation products, on stainless steel and aluminum surfaces. The anhydrous and fully wetted (0001) α-Al_2O_3 and α-Cr_2O_3 surfaces were taken as models for aluminum and stainless steel surfaces, respectively. Only on the anhydrous surfaces, a clear ranking in adsorption energy is observed: carboxylic acid > methyl esters > alcohol ~ketone > aromatics > alkanes. The different surfaces reactivity range in the order anhydrous Al_2O_3 > anhydrous Cr_2O_3 > ~hydroxylated Al_2O_3 and Cr_2O_3. Calculated desorption temperatures show that only on aluminum-based surfaces some of the investigated organic molecules remain adsorbed at operational conditions (500 K).

1. Introduction

Biodiesel use has increased in the transport sector (WEO, 2017) since it is one of the main levers to reduce the transportation CO_2 fingerprint on the environment. Biodiesel is mainly composed of fatty acid methyl esters (FAME) which are known to be easily degraded in injection systems conditions (Alves Fortunato et al., 2019). In Europe, rapeseed methyl ester (RME) is the most used biodiesel in the market (WEO, 2017) and it is mainly composed of oleate methyl ester ($C_{18:1}$).

One of the main concerns about biodiesel use is its tendency towards oxidation at low temperatures (<300 °C), also called autoxidation process, as well as its low thermal stability (Corporan et al., 2011; Grinstead and Zabarnick, 1999). Both processes can lead to fuel degradation due to the formation of deposits on the metallic surfaces being in contact with the fuel, which in turn leads to fouling of the injection systems causing powertrain performance reduction (Richter et al., 2013; Barker et al., 2014). Understanding the role of molecular interactions between biodiesel molecules with metallic surfaces is of ubiquitous importance to predict and enhance fuel system performances. The metal/alloy surfaces of our concern are stainless steel and aluminum as they are largely used in injection systems. The temperature of the injector in fuel systems can achieve 150 °C with a water residual content of 1000 ppm under engine working conditions. At this temperature, aluminum is covered with an oxide and a hydrated film (Łodziana et al., 2003). Indeed, the work of Kenza Bacha (Bacha, 2016) showed using X-ray Photoelectrons Spectroscopy (XPS) that the aluminum surfaces can present oxides and hydroxides on the upper surface. The same is true for stainless steel, which is covered with a hydroxylated chromia layer as shown by experimental (Massoud et al., 2014; Bikondoa et al., 2010; Lübbe and Moritz, 2009; Bender et al., 1995) and theoretical studies (Souvi et al., 2017; Arrouvel et al., 2007; Costa et al., 2009; Gouron et al., 2015; Nigussa et al., 2011). For the latter studies, aluminum/aluminum oxide surfaces are generally simulated by model oxides like α-Al_2O_3 (Siegel et al., 2002; Renaud, 1998; Baran et al., 2014), or γ-Al_2O_3 (Costa et al., 2014). These oxide models have, in turn, been used to notably study adsorption processes like water (Arrouvel et al., 2007; Wittbrodt et al., 1998; Wang et al., 2000; Di Felice and Northrup, 1999; Tepesch and Quong, 2000; Hass et al., 1998; Arrouvel et al., 2004a, 2005, 2004b; Borck et al., 2007; Borck and Schröder, 2006a; Chakarova-Käck et al., 2006; Borck and Schröder, 2006b; Pan et al., 2008, 2010; Wang et al., 2017; Jenness et al., 2014; Shukla and Hill, 2013; Kistamurthy et al., 2016; Wischert et al., 2012; Xu et al., 2014; Digne et al., 2002; Hass et al., 2000; Soleymanibrojeni et al., 2020). These seminal works are taken as our starting point for our dry and fully hydrated model surfaces, representing the aluminum and stainless steel surfaces that are largely used in engine systems, to improve our understanding of both adsorption mode and energetics of different biodiesel oxidation products. This will then provide a step forward towards proposals of adapted mitigation pathways.

Biodiesel oxidation products are mainly composed of molecules containing methyl esters, carboxylic acids, ketones, aldehydes, alcohols or

* Corresponding authors.
E-mail addresses: theodorus.de-bruin@ifpen.fr (T. de Bruin), dominique.costa@chimieparistech.psl.eu (D. Costa).

https://doi.org/10.1016/j.rsurfi.2022.100050
Received 19 October 2021; Received in revised form 12 January 2022; Accepted 24 January 2022

epoxides as the main chemical functions (Chatelain et al., 2016; Alves-Fortunato et al., 2018; Bacha et al., 2015). Some of these oxygenated species seem to be the precursors of deposits observed in aluminum and stainless steel surfaces (Alves Fortunato et al., 2019; Richter et al., 2013; Lacey et al., 2012; Ullmann et al., 2008).

Interaction of oxygenated species on aluminum surfaces have been widely studied in the literature. Alexander et al. identified via Fourier-transform infrared spectroscopy (FTIR) the formation of bonds between carboxylic acids and hydroxylated AlOOH surfaces (Alexander et al., 2001). Lim et al. (2007) studied the adsorption and desorption of stearic acid self-assembled monolayers on aluminum oxide via XPS and IR spectroscopy analyses. They found that stearic acid makes both monodentate and bidentate bonds with the alumina surface. Hafidi et al. studied the interactions between vegetable oils (containing methyl esters) and alumina membranes by FTIR (Hafidi et al., 2004). They found that all selected lipids in their study adsorbed on alumina. The adsorption proceeds by the surface hydroxyl groups and the polar groups of the lipids, in particular tri- and di-acylglycerols species adsorb physically via H bonds through the carbonyl ester group (C=O). Oleic acid is chemically adsorbed by ionic interaction between the carboxylate anion ($RCOO^-$) and the metal oxide.

Many theoretical works have been published regarding adsorption on Al_2O_3 surfaces. Wang et al. (2017) have investigated the adsorption of methyl nitrate on dry (0001) α-Al_2O_3 and (110) γ-Al_2O_3. They found that the adsorption on (110) surface is more stable than on α-Al_2O_3. A Density Functional Theory (DFT) study by Kistamurthy et al. (2016) showed the dissociative adsorption of acetic acid on the (100) and (110) γ-Al_2O_3 anhydrous surfaces, where both oxygen atoms of the acetate coordinate to the surface. Heiden et al. (2019) calculated with PBE-D3 a value of −157.3 kJ mol^{-1} for the dissociative and −124.5 kJ mol^{-1} for molecular water adsorption on α-Al_2O_3(0001) (1/4 ML coverage on a (2 × 2) surface). Borck and Schröder (2006b) studied the methanol adsorption at the (0001) surface of α-Al_2O_3. They found that the adsorption mechanism is a donor–acceptor interaction, where the methanol's oxygen lone pair orbital donates electron density into Al conduction band. Arrouvel et al. (2007) have studied the glycine adsorption on anhydrous and hydroxylated (0001) surfaces of α-Al_2O_3 showing that on the dry surface, the glycinate anion forms an iono-covalent Al-OC bond and it is stabilized in a unidentate perpendicular configuration with an adsorption energy of −214 kJ mol^{-1}. In the case of the hydroxylated surface, it is observed that the substitution of a surface OH group by glycine is thermodynamically favored (ΔE_{ads} = −213 kJ mol^{-1}). The adsorption of CO_2 on γ-alumina using DFT has been studied by Pan et al. (2008, 2010) they also found that the adsorption energy decreased when the water coverage increased in agreement the previously mentioned studies. Recently, Blanck et al. (2020) studied the solvation and adsorption properties of various species of lubricant additives to investigate the most suitable among them that favors the wetting of γ-alumina surface. From their results, Blanck et al. (2020) ranked the reactivity of the protic molecules (e.g. alcohols and carboxylic acids) correlating their adsorption energies with the pKa value in water, finding that the carboxylic acid > alcohol in terms of adsorption energy on (100) γ-alumina surface.

Soleymanibrojeni et al. (2020) performed MD simulations using ReaxFF to the interaction of Diglycidyl Ether of Bisphenol-A (DGEBA) with the hydroxylated (001) γ-alumina. They found that the interaction energies of the epoxy with water are greater than those of epoxy with Al_2O_3 and that interaction energies of epoxy with the substrate decrease by increasing the number of water molecules.

Concerning stainless steel surfaces, less literature data is available on DFT/ab-initio principles approaches. The adsorption of CO_2 on different Cr_2O_3 surfaces terminations (0001), (0112) and (1012) was studied by Kumar et al. (2020). They found that CO_2 can either physisorb or chemisorb on Cr_2O_3 surfaces. Also, CO_2 chemisorption on the Cr_2O_3 (1012) surfaces exhibits an E_{ads} = −103.2 kJ mol^{-1} that is very close to the experimental values (−104.2 kJ mol^{-1}).

Costa et al. (2009) studied water adsorption on the (0001)-Cr_2O_3-Cr terminated facet and found that molecular and dissociative adsorption were isoenergetics with values of −82.2 (dissociative) and −82.6 (molecular) kJ mol^{-1}. For three water molecules adsorbed per Cr, the average adsorption energy was calculated as −93.2 kJ mol^{-1}. Souvi et al. (2017) calculated an adsorption energy of −80.3 kJ mol^{-1} for dissociative water adsorption (more stable than the molecular one). At saturation (3 water molecules per Cr), the average adsorption energy was calculated as −87.9 kJ mol^{-1}. Matthew et al. (2018) studied water adsorption on Cr_2O_3 with DFT+U and found that the adsorption energy of the first water is 96.5 kJ mol^{-1}, for 80.1 kJ mol^{-1} average adsorption energy at saturation.

Gouron et al. (2015) studied by DFT the adsorption of monoethanolamine (MEA) on the hydroxylated Cr_2O_3 (0001) orientation where it follows that MEA adsorbs in a bidentate fashion, preferentially on top of the water molecules forming the hydroxylated surface, while the water substitution is thermodynamically not favorable at room temperature. Ethanol adsorption on Cr_2O_3 (0001) was studied by Zhang et al. (2014) and found to be exothermic by 90.7 kJ mol^{-1}. However, the authors performed DFT calculations without explicit dispersion corrections. Huš et al. (2020) studied the adsorption of propane on dry (0001) Cr_2O_3 with DFT+U including van der Waals forces described by Grimme D3 method (Grimme et al., 2010). According to their results, the adsorption energy for propane on dry (0001) Cr_2O_3 is −34.7 kJ mol^{-1}. Benzene was adsorbed on s-type surfaces (Dabaghmanesh et al., 2016) . The adsorption energy was calculated as −50.2 and −53.1 kJ mol^{-1} for dry Cr_2O_3 and Al_2O_3, respectively.

Acetic acid was chosen as a model molecule of biofuels in a DFT based study and was adsorbed on Co stepped surfaces (Li et al., 2015). Co-O and Co-C bonds were formed, with an adsorption energy of −75 kJ mol^{-1}.

To make a step forward towards more realistic systems, including the liquid phase/surface interaction, classical molecular dynamics (MD) studies have been performed. Adsorption of a model fuel composed of n-tetradecane containing 0 to 5% ester on iron (taken as model of steel) was studied with molecular dynamics (Mei et al., 2020). The adsorption energy of the fuel on the surface was shown to increase with the ester amount in the fuel. For fuel blends containing saturated esters, the adsorption energy of the film rises with the increase of the carbon chain length, while for fuel blends containing unsaturated esters it remains at the same level.

Whereas MD studies of fuels/surfaces are still emerging, certainly due to the complexity of biofuels composition and diversity of reaction products, we also refer here to some MD studies performed in the field of adhesion and protection. Adhesive molecules are often composed of epoxy polymers, which are of interest with respect to this study since small epoxy molecules were already identified as a product of autoxidation of biofuels molecules (Bacha, 2016; Alves-Fortunato et al., 2018). The adsorption of epoxy coating on different types of iron oxides, which naturally exist on steel substrate, was studied via MD simulations (Bahlakeh et al., 2016). Three types of iron oxide, that is, ferrous oxide (FeO), ferric oxide (Fe_2O_3, hematite), and ferrous ferric oxide (Fe_3O_4, magnetite), were considered for modeling, and their binding energies were calculated and compared by altering the concentration of hydroxide groups on the surface. The authors showed that the epoxy was bound to the surfaces through electrostatic and donor–acceptor interactions. Moreover, they found that more hydroxylated the surface, higher the adhesion energy of the epoxy with the surface, thanks to the formation of N and O bonds with surface OH groups. They mention a synergetic aspect of H bond and N and O species-iron donor–acceptor interaction.

Epoxy resins were also adsorbed on metal Fe, (taken as a model of steel), in order to investigate their corrosion protection power (Hsissou et al., 2021; Hsissou, 2021; Hsissou et al., 2020a,b). The studied macro-molecules were heterocyclic epoxy resin triazine (Hsissou et al.,

2021), pentaglycidyl ether pentabisphenol A of phosphorus (PGEPBAP) (Hsissou et al., 2020a) and triglycidyl ether tribisphenol A of ethylene (TGETBAE) (Hsissou et al., 2020b), hexaglycidyl trimethylene dianiline of ethylene (HGTMDAE), pentaglycidyl ether pentaphenoxy of phosphorus (PGEPPP), and decaglycidyl pentamethylene dianiline of phosphorus (DGPMDAP) (Hsissou, 2021). In all cases, the calculations suggest that adsorption of the macromolecule is parallel to the surface, enhancing the hetero-atom of the macro-molecular matrix and -Fe. The epoxy adsorbs parallel to the iron surface both in HCl and H_2SO_4 medium, and at 298 and 328 K, suggesting that the epoxy-metal interaction is maintained with a moderate increase of temperature (Hsissou et al., 2021). As shown by the authors, Fe-C, Fe-O and Fe-N bonds formation are observed. For TGETBAE, the MD simulation reveals that O and C atoms of the macromolecule form both chemical bonds (characterized by Fe-O, Fe-C distances < 3.5 Å) and physical interactions (Fe-O, Fe-C distances between 3.5 and 7 Å) with surface Fe (Hsissou et al., 2020b).

These systems are very different from the biofuel-stainless steel/aluminum ones we are interested in, both considering the nature of the surface and of the liquid phase, nonetheless, information on molecule–surface interactions and on molecule–surface interaction in the presence of water are provided.

A last mention to be considered is indeed the role of water in organic matter adsorption. Whereas it is largely accepted that hydroxylation/hydration plays a key role in molecule adsorption, few experimental studies have scrutinized the effect of water loading on this molecular adsorption. For example, the gaseous formic acid adsorption on clays at decreasing relative humidity was performed (Rubasinghege et al., 2013). The co-adsorption/desorption phenomena of carboxylate on goethite was recently evidenced with Fourier transform IR spectroscopy (FT-IR) microscope through cycles of dehydration/rehydration, and confirmed using DFT (Botella et al., 2021).

To summarize, the overview of the literature shows that modeling approaches of biofuel surfaces are still in the infancy. First principles methods are used to estimate the binding energy and bonding mode of several molecules — that are of interest in our study, as models of precursors of autoxidation products, on different surfaces. Several studies evidence the possibility of oxygenated molecules to displace adsorbed water and form a direct bond with a metal atom at the surface. Finally, classical MD studies on organic molecules evidence the interaction between the surface atoms and atoms of the macromolecules as –C, -O. Summarizing, systematic studies of diverse molecule families and on several substrates, at various hydration degree, are scarce.

In the present paper, we thus undertook a systematic DFT study of small molecules (taken as model of biofuels) adsorption on two model surfaces, Al_2O_3 and Cr_2O_3 (taken as models of aluminum and stainless steel). We examine the adsorption energies on the dry and hydroxylated surfaces.

2. Methodology and models

2.1. Computational details

Total energy calculations were performed within the density functional theory (DFT) and the generalized gradient Pedrew–Burke–Erzenhoff (PBE (Perdew et al., 1996)) exchange correlation functional was used for the whole study. To solve the Kohn–Sham equations we use the Vienna Ab initio Simulation Package (version 5.4.1) (Kresse, 1993; Kresse and Hafner, 1994; Kresse and Furthmuller, 1996; Kresse and Furthmüller, 1996). VASP performs an iterative diagonalization of the Kohn–Sham Hamiltonian via unconstrained band-by-band minimization of the norm of the residual vector to each eigenstate and via optimized charge density mixing routines. A smearing of 0.1 eV was used. We used a cut-off energy of 520 eV for the total energy calculations. The electronic optimizations were done up to a convergence of 10^{-5} eV for the self-consistent loop and until all forces on the atoms were lower than 0.02 eV/Å for the geometry relaxations. The Brillouin zone was sampled with an appropriated Monkhorst–Pack] **k**-point mesh (*vide infra*) (Monkhorst and Pack, 1976).

To account for the strong correlation between the d-electrons of the chromium, an on-site coulomb repulsion U-term is added to the DFT Hamiltonian, turning into DFT + U method. (Anisimov et al., 1997) Subsequently, this formalization impacts on the cell dimensions, band gap and, magnetic moment. Herewith, we have considered U and J parameters to be 5 eV and 1 eV respectively as reported in the literature. (Souvi et al., 2017; Rohrbach et al., 2004) To account for the antiferromagnetic state of Cr_2O_3, spin-polarized calculations were performed.

The Van der Waals corrections are calculated with DFT-D3 method of Grimme (Grimme et al., 2010) at each electronic step, implying that the geometry is optimized with the dispersion forces included.

2.1.1. Relative energy calculations

We calculated the adsorption energy ($\mathbf{\Delta E_{ads}}$) according to the following equation:

$$\mathbf{\Delta E_{ads} = E_{molecule+slab} - E_{molecule} - E_{slab}} \quad (1)$$

where $\mathbf{E_{molecule+slab}}$ is the total energy of the optimized structure formed after the molecule is (chemically) absorbed on the oxide slab and $\mathbf{E_{molecule}}$ and $\mathbf{E_{slab}}$ are the total energies of the non-interacting molecule, respectively, the slab.

Furthermore, the adsorption energy has been decomposed in two contributions: the $\mathbf{E_{ads}^{vdW}}$ energy resulting from the dispersion interactions (as calculated using Grimme's zero damping DFT-D3 method (Grimme et al., 2010)), and the "pure" DFT energy ($\mathbf{E_{ads}^{DFT}}$), which corresponds to DFT total energy computed using a given exchange correlation functional as defined in Eq. (2) below:

$$\mathbf{\Delta E_{ads}^{DFT} = \Delta E_{ads} - \Delta E_{ads}^{vdW}} \quad (2)$$

The adsorption of a molecule with an acidic proton (RH, R being a radical, R = $CH_3COO°$) may result in a surface OH substitution following an acid base mechanism:

$$\mathbf{RH + Slab - HY(-OH_s) \rightarrow Slab - R + H_2O} \quad (3)$$

where **Slab-HY** is the hydroxylated surface and the **(–OHs)** coincides with the substituted –OH surface termination (Fig. 1).

In reference to the adsorption mechanism for this dissociative configuration, what happens between the acetic acid and the OH_s can be described as a Brønsted-Lowry reaction reported in Fig. 1 below, where the acetic acid represents the proton donor (Brønsted-Lowry acid) and the OH_s represents the proton acceptor (Brønsted-Lowry base). In fact, when the acetic acid reacts with the OH_s through the H atom of its hydroxyl group, the result is the formation of its conjugate base (acetate) and of a released water molecule.

The substitution energy $\mathbf{\Delta E_{subst}}$ was calculated as:

$$\mathbf{\Delta E_{subst}(RH) = E_{slab-R} - E_{RH} - E_{Slab-HY(-OH_s)} + E_{H2O}} \quad (4)$$

For the methyl propionate (MP) case, instead of the substitution of a superficial –OHs, we preferred to study the substitution of an entire chemisorbed water molecule at the surface; in this case, we have:

$$\mathbf{MP + Slab - HY(-OH_{2s}) \rightarrow Slab - MP + H_2O} \quad (3')$$

and

$$\mathbf{\Delta E_{subst} = E_{slab-MP} - E_{MP} - E_{Slab-HY(-OH_2s)} + E_{H_2O}} \quad (4')$$

where in this case the **Slab-HY** is characterized by a chemisorbed water termination ($\mathbf{-OH_{2s}}$).

We can analyze further these results in calculating the different components of the substitution energy: water desorption energy and

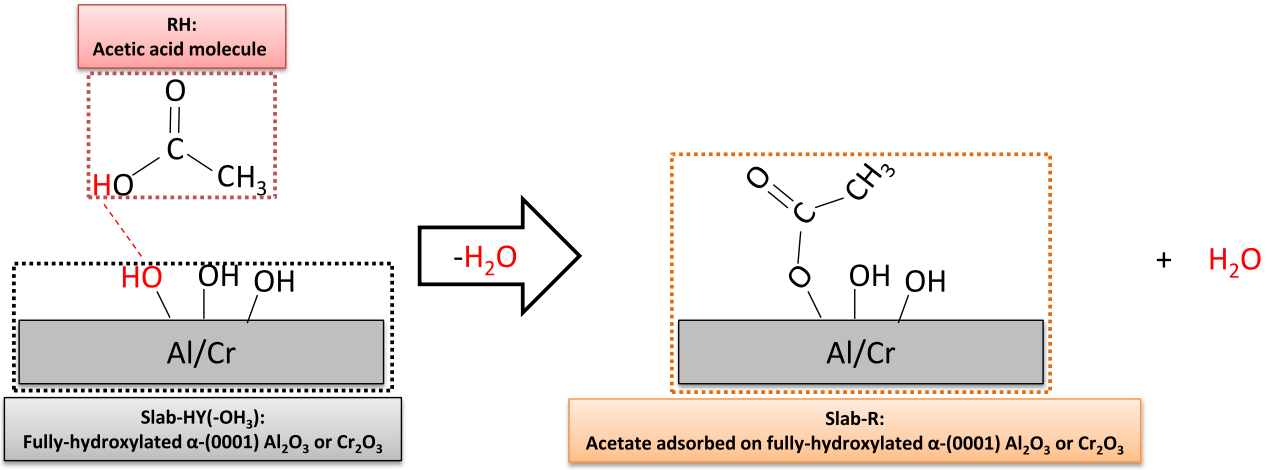

Fig. 1. Simplified scheme for the substitution OH reaction with an acetate molecule described as a Brønsted-Lowry reaction.

molecule/surface binding energy. We have, if X is the adsorbed moiety, either R or MP,

$$\Delta E_{subst} = \Delta E^{desorb}_{H_2O} + E^{binding}_{Slab-X} + \Delta E^{relaxation}_{Slab-HY-minus-H_2O} \quad (5)$$

With

$$\Delta E^{desorb}_{H_2O} = E_{Slab-HY-minus-H_2O} - E_{Slab-HY} + E_{H_2O} \quad (6)$$

And

$$E^{binding}_{Slab-X} = E^{optimized}_{Slab-X} - E_X - E^{geometry\ if\ X\ is\ adsorption}_{Slab-HY-minus-H_2O} \quad (7)$$

And

$$\Delta E^{relaxation}_{Slab-HY-minus-H_2O} = E^{optimized}_{Slab-HY-minus-H_2O} - E^{geometry\ if\ X\ is\ adsorption}_{Slab-HY-minus-H_2O} \quad (8)$$

On the basis of the adsorption energies, we estimated the desorption temperatures as the temperature where $\Delta G_{ads} = 0$ or $\Delta H_{ads} = T\Delta S_{ads}$. Assuming that $\Delta H_{ads} \approx \Delta E_{ads}$ and that the loss in entropy upon adsorption is solely due to the complete loss of translational and rotational entropy, while $\Delta S_{vib} = 0$, the desorption temperature equals:

$$T_{desorb} = -\Delta E_{ads}/(S_{trans} + S_{rot}) \quad (9)$$

Where S_{trans} and S_{rot} are respectively the translational and rotational entropy contributions of the adsorbate in the gas phase. These entropic contributions were calculated at T_{desorb} at the B3LYP/6-311G(d,p) level with Gaussian 16 (Frisch et al., 2016). Further details are reported in the Supplementary material.

2.2. Model of surrogate

As previously discussed, the main products sorted out from fuel autoxidation are oxygenated compounds like alcohols, aldehydes, ketones, epoxides and carboxylic acids. Based on the previous experimental work of K. Bacha (Bacha, 2016), the XPS results of real biofuels deposits over different surfaces (alumina, stainless steel, gold, polymer) showed that the chemical bond between deposits and surface was made through the oxygenated head of the molecule under study. In addition, the study conducted by Mei et al. (2020) showed that the increase of the adsorption energy of the fuel on the surface was exclusively dependent of the ester amount in the fuel. For these reasons, in the present study small oxygenated molecules have been preferred as model molecules on the basis of their chemical functional group, i.e. ethanol for the alcohol family, acetaldehyde and acetone to represent aldehydes and ketones respectively, 2-ethyl-3-methyloxirane for the epoxides and acetic acid for the carboxylic acids. In addition, three other types of chemical families have been considered:

(1) aromatic species since they are one of the main components of diesel refined from crude oil, and so they are present in the diesel/biodiesel blends in the market, here we consider benzene and toluene as model aromatic compounds.

(2) ester species: methyl propionate, unsaturated methyl esters (e.g. methylacrylate and methyl-3trans-hexenoate), as representatives of deposits derived from biodiesel blends.

(3) alkanes since they are the main component of fuels in general, here we consider n-propane as surrogate of alkyl-chain deposits produced from n-alkanes degradation.

The listed model molecules are reported in Table 1 below, where they have been matched with the corresponding configuration optimized via DFT (last right column):

2.3. Bulk oxides

The rhomboidal (R3c) unit cells of α-Al_2O_3 and α-Cr_2O_3 according to X-ray data were taken as the starting point for the calculations of the bulk oxide. For the corundum-type surfaces, the hexagonal unit cell used in this study (cf. Fig. S1 in Supplementary Materials) is built from three (rhomboidal) subunits, each containing 4 metal cations. Each subunit can have three spin configurations leading to an antiferromagnetic configuration: A (+ + − −), B (+ − − +) and C (+ − + −). We agree with Rohrbach et al. (2004) and Costa et al. (2009) that the hexagonal cell Cr_2O_3, containing 3 subunits, with spin configuration (CCC), reflects the spin ground state and results in a total magnetic moment of zero. The **k**-point grid was optimized for each system and electronic energy convergence was obtained with **k**-points grids of (3 × 3 × 1) for α-Al_2O_3 and α-Cr_2O_3. The unit cell was relaxed by alternating a cell parameter optimization and ion relaxation until convergence criteria for the forces and energies were obtained (*vide supra*). The results are shown in the Supplementary material Tables SI-S1 and S2.

2.4. Surfaces

For α-alumina and α-chromia, both the Al(Cr)-terminated dry surface (Bulk-Al–O–Al) (respectively Bulk-Cr–O–Cr) and the fully hydrated Bulk-Al-O-Al-$(OH)_3$/ and Bulk-Cr-O-Cr-$(OH)_3$/surfaces were considered (see Supplementary material Fig. S1). The oxide slab thicknesses correspond to seven and eight layers, respectively. We validated our calculation methodology, by verifying that for the dry surfaces, the calculated surface energy of α-Al_2O_3 1.55 J/m^2 is in good adequacy with the literature (Arrouvel et al., 2007) value of 1.66 J/m^2.

The lattice parameters and surface areas for the examined surfaces are grouped in Table 2. The values for the **k**-point mesh have been

Table 1
Organic molecules selected as models for representing the precursors of the liquid deposits coming from the fuel autoxidation process.

Chemical family	Model molecule	Chemical structure
Alcohol	ethanol	
Aldehyde	acetaldehyde	
Ketone	acetone	
Epoxide	2-ethyl-3-methyloxirane	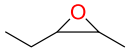
Carboxylic acid	acetic acid	
Aromatic compounds	benzene	
	toluene	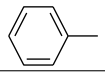
Methyl esters	methylacrylate	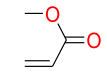
	methyl-3-trans-hexenoate	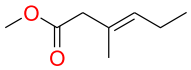
	methyl propionate	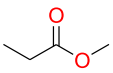
Alkane	n-propane	

Table 2
Lattice parameters for the DFT computed (4 × 4) slabs for α-Cr_2O_3(001) and α-Al_2O_3(001) respectively.

Surface (4 × 4) slab	Size	a-axis in supercell [Å]	b axis in supercell [Å]	Number of layers	Area surface supercell [Å^2]	Slab thickness [Å]	Vacuum thickness [Å]	K-points mesh
α-Cr_2O_3(0001)	4 × 4	20.29	20.29	6	356.58	13.85	14.59	1 × 1 × 1
α-Cr_2O_3(001)-$Cr(OH)_3$	4 × 4	20.29	20.29	7	356.58	15.27	13.17	1 × 1 × 1
α-Al_2O_3(001)	4 × 4	19.14	19.14	6	317.25	13.07	14.51	1 × 1 × 1
α-Al_2O_3(001)-$Al(OH)_3$	4 × 4	19.14	19.14	7	317.25	14.71	12.86	1 × 1 × 1
α-Cr_2O_3(0001)-$Cr(OH)_3$	2 × 2	10.15	10.15	6	89.15	15.27	13.17	2 × 2 × 1
α-Al_2O_3(0001)-$Al(OH)_3$	2 × 2	9.57	9.57	6	79.31	14.72	12.86	2 × 2 × 1

selected in order to keep the same calculation level as that used when studying the bulk.

For the α-Cr_2O_3(0001)-Cr and α-Al_2O_3(0001)-Al surfaces, we considered a supercell (4 × 4) large enough to adsorb molecules without lateral interactions. Seen the large size of the cells, the calculations were performed at the Gamma point.

The fully hydrated α-Al_2O_3-$Al(OH)_3$ termination, corresponding to 8.7 OH/nm^2, was considered stable over a large temperature and partial water pressure range, based on the ones reported in the literature (Łodziana et al., 2003). According to Ranea et al. (2009), the final configuration $Al(OH)_3$ generated from three successive water dissociations shows an approximately trigonal coordination on the Al_s center and its formation energy from the dry surface is calculated to be –139.9 kJ mol^{-1}. A (4 × 4) cell was used, at the exception of the study of the substitution of water (OH) by methyl propionate (respectively acetate) which was performed on (2 × 2).

It should be noticed that in all molecule/surface interactions calculations only the four top layers were relaxed.

2.5. Adsorption of molecules at surfaces

To rigorously compare the reactivity of both corundum-type surfaces, the starting adsorption configurations of the molecules on dry surfaces have been maintained identical.

First, we started our study by experimenting different molecule positions and orientations above the oxide surfaces. In fact, some of the smaller molecules (such as ethanol, acetone and acetaldehyde) were placed in a tilted fashion on top of the surface by promoting a stronger interaction between the molecule O atom and the metallic surface layer and, at the same time, by allowing the molecule hydrocarbon chain to also interact with the surface layer through weaker dispersion forces.

For flatter molecules such as the aromatic compounds, we opted to arrange them parallel to the surface layer in order to favor van der Waals interactions, which are prominent for apolar molecules.

In the case of bigger molecules, as methyl-3trans-hexenoate and the 2-ethyl-3-methyloxirane, we chose to arrange them perpendicular to the surface in a monodentate adsorption configuration, in this way

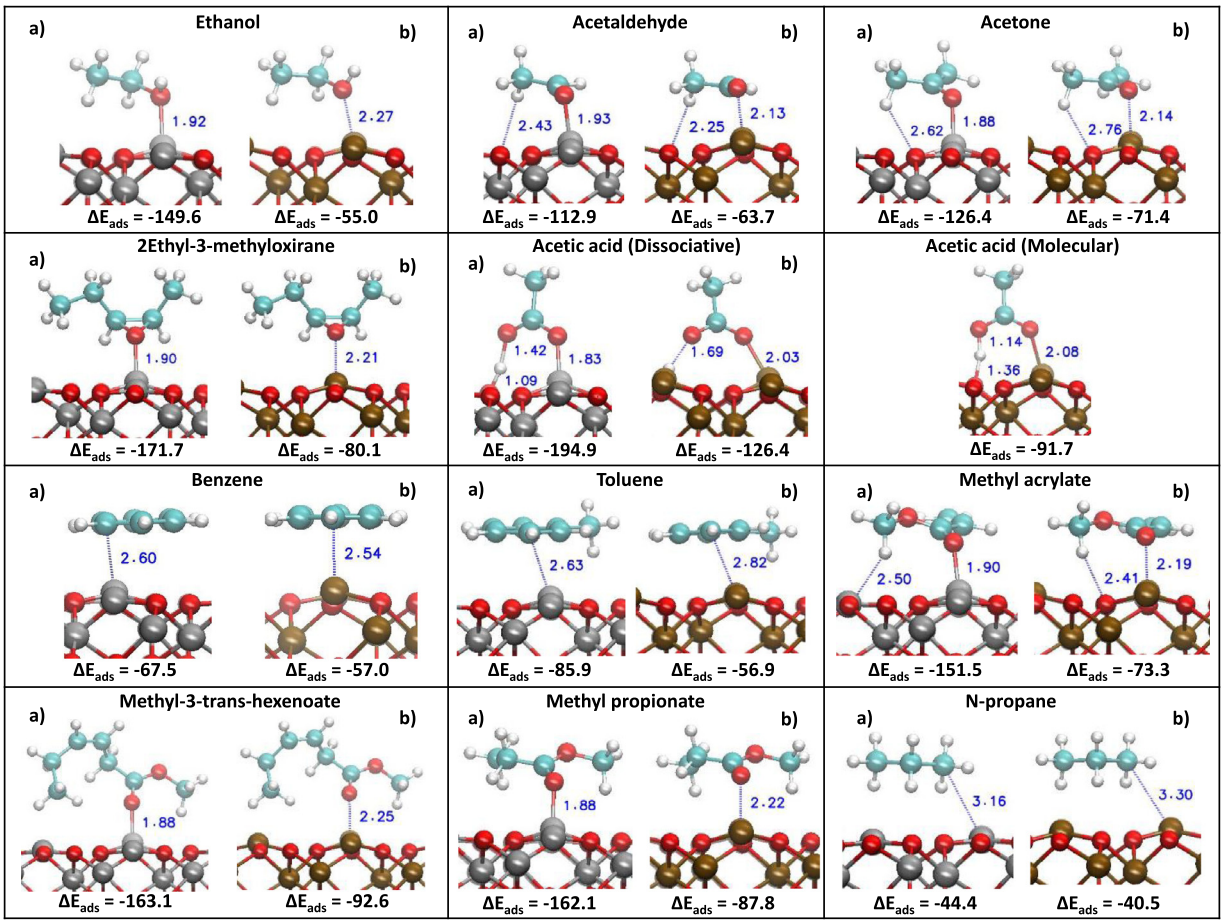

Fig. 2. Optimized adsorption configurations on anhydrous surfaces with their corresponding adsorption energies calculated via DFT approach of different model molecules on dry α-Al_2O_3 (a) and α-Cr_2O_3 (b) surfaces, respectively. The bond distances are reported in Angstrom [Å] and adsorption energies in [kJ mol^{-1}]. Color code: red = O; light-blue = C; white: H; gray = Al; brown = Cr.. (For interpretation of the references to color in this figure legend, the reader is referred to the web version of this article.)

favoring the bonding between the adsorbate O atom and the outermost M cation.

In the case of dissociative adsorption, for both dry surfaces, the dissociated adsorption configuration was formed by imposing from the beginning the transfer of the H atom on a O_s atom on the surface outermost layer. Several locations of the proton on surface oxygen atoms were considered and the most stable are retained here.

A similar reasoning has been done to study the adsorption on the hydroxylated corundum-type surfaces, since we wanted to explore the difference in reactivity of both substrates under the same conditions of hydroxylation state and organic adsorbates. As a starting point, the molecules were placed in a similar position as that obtained on the anhydrous surfaces, but farther from the surface.

3. Results

3.1. Adsorption on dry α-Al_2O_3 and α-Cr_2O_3 surfaces

Fig. 2 shows the optimized geometries obtained for the molecules on the dry corundum-type surfaces α-Al_2O_3(a) and α-Cr_2O_3(b), respectively. From Fig. 2 it appears that the final configurations are very similar for Al_2O_3 and Cr_2O_3. For both metal-oxide surfaces the strongest interactions are represented by the metal-oxygen covalent bonds that are formed between the oxygenated polar groups (hydroxyl and carbonyl groups), acting as a Lewis base, of the adsorbate and the metallic atoms (Al/Cr), terminating the surfaces, acting as Lewis acids.

Apolar molecules such as alkanes (n-propane) and aromatic compounds (benzene and toluene) do not form covalent bonds with the oxides and essentially associate by induction and dispersion forces. Indeed, the Al-C and Cr-C bonds formed are 2.60 and 2.54 Å respectively, suggesting weak interactions. These values are in good agreement with those calculated by Alexander et al. (2001), 2.82 and 2.68 Å respectively. The adsorption energies calculated by the authors, −53.1 kJ mol^{-1} and −50.2 kJ mol^{-1} for Al_2O_3 and Cr_2O_3, are also in good correlation with our calculations, −67.5 and −57.0 kJ mol^{-1}.

For water and acetic acid, both the associative (molecular) and dissociative adsorption have been considered (Fig. 3). On Al_2O_3 the non-dissociative adsorption evolves during the geometry optimization towards a dissociative adsorption, through a proton transfer to a surface O atom (see Fig. 2). For the chromia case, acetic acid can adsorb molecularly and dissociatively, the second case being more exothermic by 34.7 kJ mol^{-1}. The barrier from the molecular to the dissociative adsorption was evaluated to 20.3 kJ mol^{-1} (the barrier was calculated using the Nudged Elastic Band approach).

We considered for the Al_2O_3 surface two different dissociative configurations: the "1–2" dissociation for water and the "1–4" dissociation for acetic acid, *cf*. Fig. S2 in the Supplementary material for the nomenclature. It appears that a small molecule like water, preferentially adsorbs in the 1–2 position, in agreement with literature data (Hass et al., 1998), while for the larger acetic acid, the 1–4 position is most stable. In fact, the 1–2 (respectively 1–4) position maximizes the hydrogen bond interactions between the O from the OH (respectively COO) group and the adsorbed proton.

We report in Fig. 3a the comparison between their initial configurations, in this way highlighting the differences in their calculation starting points. From Fig. 3a, we find the dissociation of the acetic acid

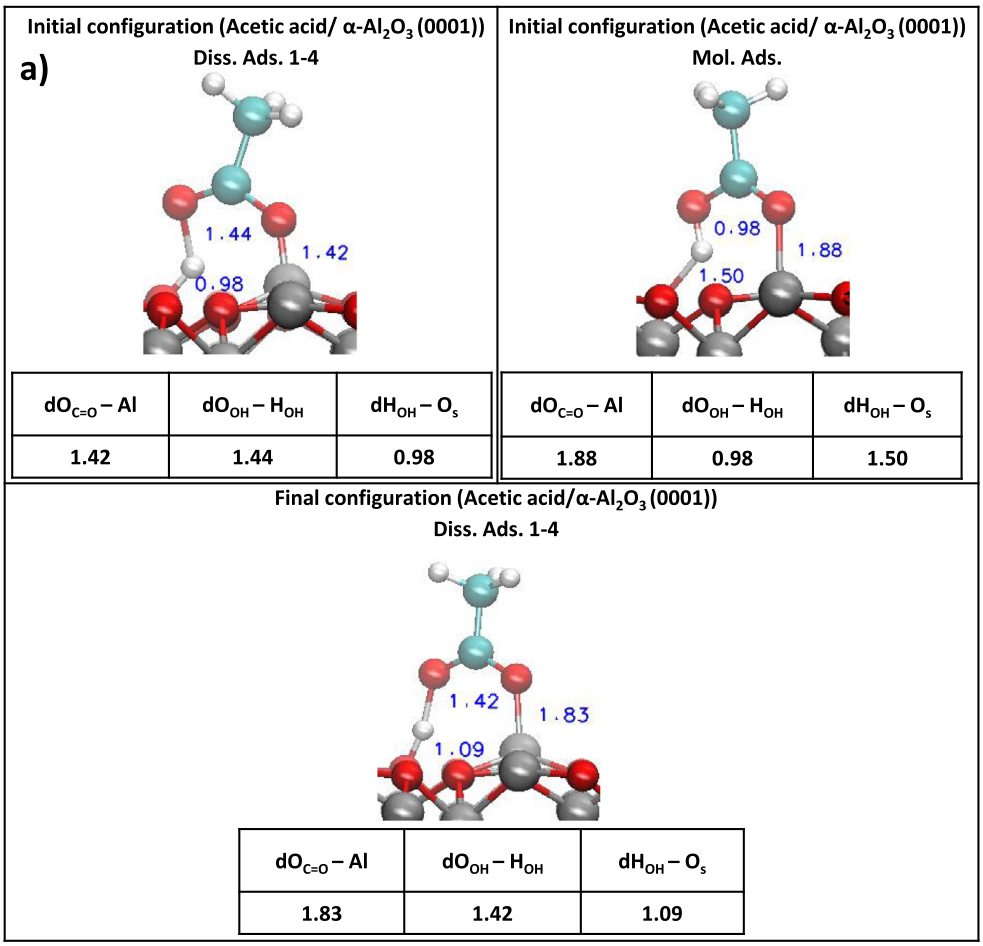

$dO_{C=O} - Al$	$dO_{OH} - H_{OH}$	$dH_{OH} - O_s$
1.42	1.44	0.98

$dO_{C=O} - Al$	$dO_{OH} - H_{OH}$	$dH_{OH} - O_s$
1.88	0.98	1.50

$dO_{C=O} - Al$	$dO_{OH} - H_{OH}$	$dH_{OH} - O_s$
1.83	1.42	1.09

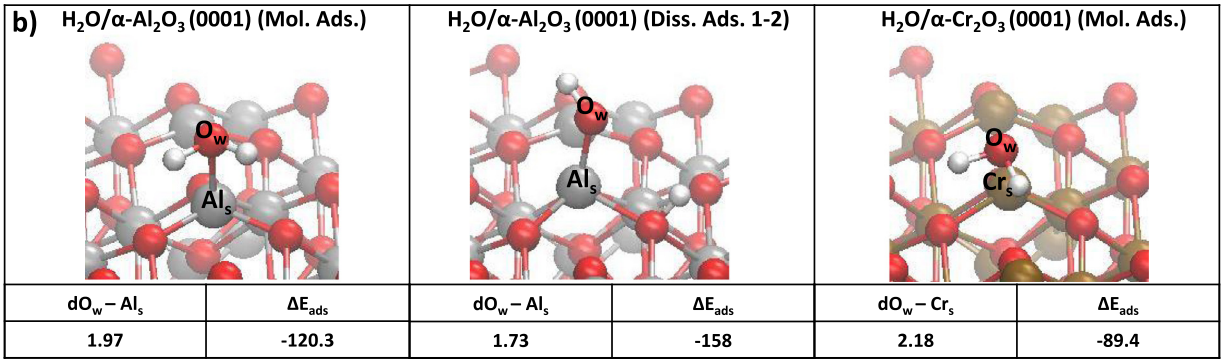

$dO_w - Al_s$	ΔE_{ads}	$dO_w - Al_s$	ΔE_{ads}	$dO_w - Cr_s$	ΔE_{ads}
1.97	-120.3	1.73	-158	2.18	-89.4

Fig. 3. (a): Starting and final configurations of the acetic acid dissociative 1–4 and molecular adsorptions on dry α-Al_2O_3. (b): configurations of the water dissociative and molecular adsorptions on dry α-Al_2O_3 and Cr_2O_3. The bond distances are reported in Angstrom [Å] and the adsorption energies in [kJ mol^{-1}]. Color code: red = O; light-blue = C; white: H; gray = Al; brown = Cr.. (For interpretation of the references to color in this figure legend, the reader is referred to the web version of this article.)

on dry α-Al_2O_3 also in the molecular adsorption case, leading us to the conclusion that the acetic acid spontaneously dissociates on α-Al_2O_3. However, the same cannot be said for the acetic acid adsorbed on α-Cr_2O_3 (Fig. 2), where the dissociative and associative configurations show a marked difference in terms of adsorption energies (−126.4 kJ mol^{-1} for the dissociative case against −91.7 kJ mol^{-1} for the associative case) and also in terms of bond lengths.

For water, (Fig. 3b) we calculated associative and dissociative adsorption energy that fit well with the literature data: −158 and −120.3 kJ mol^{-1} for dissociative and molecular adsorption of water on Al_2O_3 (Heiden et al., 2019), and around 90 kJ mol^{-1} for water (molecular) on Cr_2O_3 (Costa et al., 2009). We indeed found that for water adsorbed on Cr_2O_3, starting from the 1–4 dissociative adsorption, the system evolves towards the molecular adsorption mode. This result agrees with that of Costa et al. (2009), where the molecular and dissociative adsorption modes of water were found iso energetics.

Fig. 4a compares for all molecules, the adsorption energies on Al_2O_3 and Cr_2O_3. It appears clearly that Al_2O_3 is more reactive than Cr_2O_3 since it presents more negative adsorption energies for all molecules.

The M-O bond lengths formed for the O-containing adsorbates, are smaller for α-Al_2O_3 than for α-Cr_2O_3. Fig. 4b shows that the DFT energy contribution E_{ads}^{DFT} (thus without van der Waals contributions) is well correlated to the M-O bond length: the shorter the bond length, the higher the adsorption energy (in absolute value). The slopes of the trends for αAl_2O_3 and αCr_2O_3 are different. For Al, the Al-O bond is in a narrow range around 1.9 Å, and E_{ads}^{DFT} adsorption energies are strong, (between −80 kJ mol^{-1} and −160 kJ mol^{-1}), while the slope is

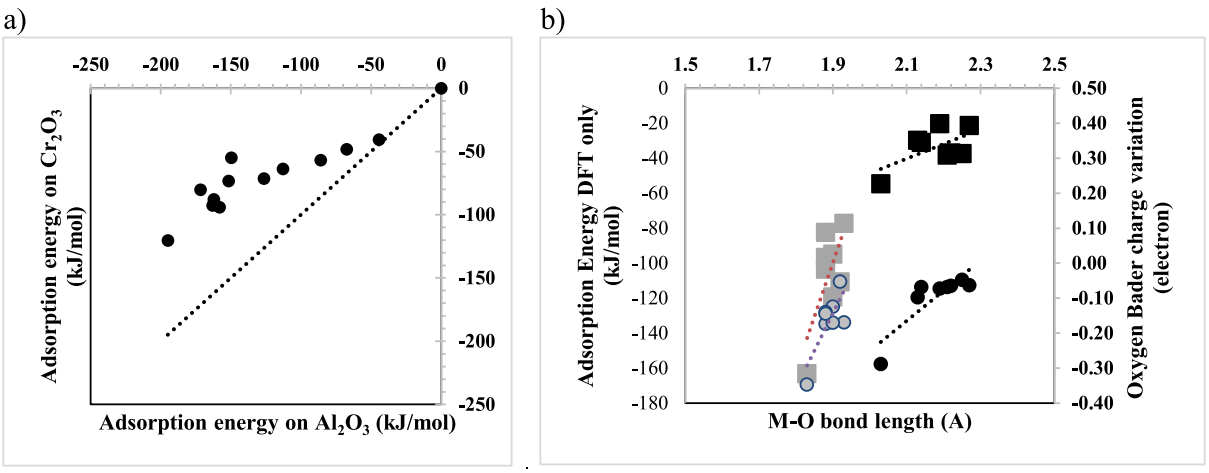

Fig. 4. (a) Adsorption energies on Cr_2O_3 versus Al_2O_3 (kJ mol^{-1}). The dashed line is the identity function (y=x). (b) DFT interaction contribution (e.g. covalent and H-bonds) plotted against Al-O (gray squares) and Cr-O (black squares) bonds respectively for oxygen-containing molecules adsorbed on anhydrous M_2O_3 (M=Al, Cr). Bader charge variation of the adsorbed O atom is reported (black circles: M=Cr; gray circles: M=Al). (For interpretation of the references to color in this figure legend, the reader is referred to the web version of this article.)

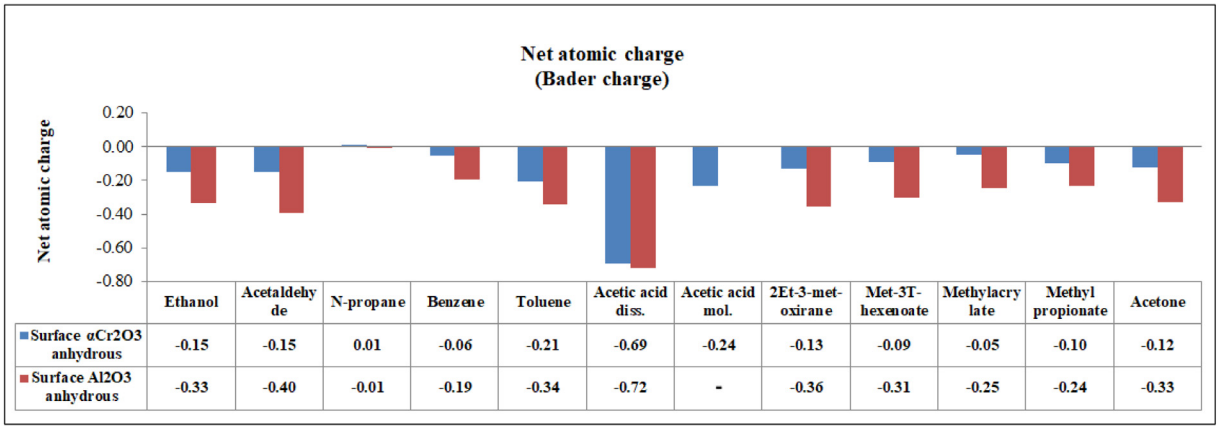

	Ethanol	Acetaldehyde	N-propane	Benzene	Toluene	Acetic acid diss.	Acetic acid mol.	2Et-3-met-oxirane	Met-3T-hexenoate	Methylacrylate	Methyl propionate	Acetone
Surface αCr2O3 anhydrous	-0.15	-0.15	0.01	-0.06	-0.21	-0.69	-0.24	-0.13	-0.09	-0.05	-0.10	-0.12
Surface Al2O3 anhydrous	-0.33	-0.40	-0.01	-0.19	-0.34	-0.72	-	-0.36	-0.31	-0.25	-0.24	-0.33

Fig. 5. Electronic charge transfer $\Delta\rho$ (electron) of the molecules adsorbed on dry α-Al_2O_3(orange) and on dry α-Cr_2O_3 (blue) respectively. A minus charge corresponds to an increase in negative charge of the molecule.. (For interpretation of the references to color in this figure legend, the reader is referred to the web version of this article.)

smoother for Cr_2O_3, where the bond length interval is larger [2.1 Å–2.3 Å] and associated with lower (in absolute value) E_{ads}^{DFT} (between −20 kJ mol^{-1} and −60 kJ mol^{-1}).

Fig. 4b also reports the charge amount transferred to O (of the organic molecule) as a function of the Al/Cr-O bonds. The electron density transferred to O (0.1 to 0.3 electron) increases with decreasing M-O bond length. In short, the more electron density is transferred, the shorter the bond length and the higher the adsorption energy. The largest electron transfer is observed for acetic acid, which in its dissociated configuration retains the charge of the lost hydrogen atom. The oxygen partial charge changes from −0.92 in neutral acetic acid in the gas phase, to −1.21 and −1.27 when adsorbed on Cr_2O_3 and Al_2O_3, respectively.

The charge transfer $\Delta\rho$ from the surface to the molecules (including molecules without oxygen) for each adsorbed molecule on dry α-Al_2O_3 and α-Cr_2O_3 is reported in Fig. 5 below. At the exception of the dissociative adsorption of the acetic acid, the charge transfer to the molecule is weak (see the detailed values in the inset below Fig. 5). For acetic acid, for which the adsorption is dissociative on alumina, the calculated charge is the charge variation of the anionic part of the molecule (the charge difference of the proton from the molecule to the adsorption on the surface is not taken into account). The charge transferred is higher (in absolute value) for Al_2O_3 than Cr_2O_3, in line with the slightly larger electropositivity (or smaller electronegativity: **X**= 1.61) of Al with respect to Cr (**X**=1.66).

In a nutshell, the molecules interact stronger with Al_2O_3 than with Cr_2O_3, as can been seen from the higher adsorption energies, the shorter bond lengths, and the higher charge transfers between molecule and Al_2O_3 with respect to Cr_2O_3.

3.2. *Adsorption on hydroxylated* α-Al_2O_3 *and* α-Cr_2O_3 *surfaces*

To understand the role of the water activity on the molecule/surface interaction, the adsorption of the molecules on the hydroxylated surfaces is discussed. Fig. 6 shows the optimized configurations obtained for the molecules on the hydroxylated surfaces. As for the dry corundum-type surfaces, we placed the molecules on top of the surface in the same initial arrangement, to compare how the same molecule interacts with the two different substrates with the same initial configuration. From Fig. 7a it is noticed that the hydration layer attenuates the adsorption energies, especially in the case of alumina. For chromia, the obtained curve is very similar to that observed for hematite by Blanck et al. (2021). The attenuation of the adsorption energy with the hydration layer depends however on the nature of the molecule–surface interaction. This is, for example, illustrated for the adsorption of ethanol. Whereas for the anhydrous surfaces adsorption energies are calculated of –149.6 and –55 kJ mol^{-1} for respectively alumina and chromia, these values reduce to practically equal values of –40.5 and –45.3 kJ mol^{-1} for the fully hydrated surfaces. Similar trends are observed for the aldehyde, ketone, epoxide and esters, which

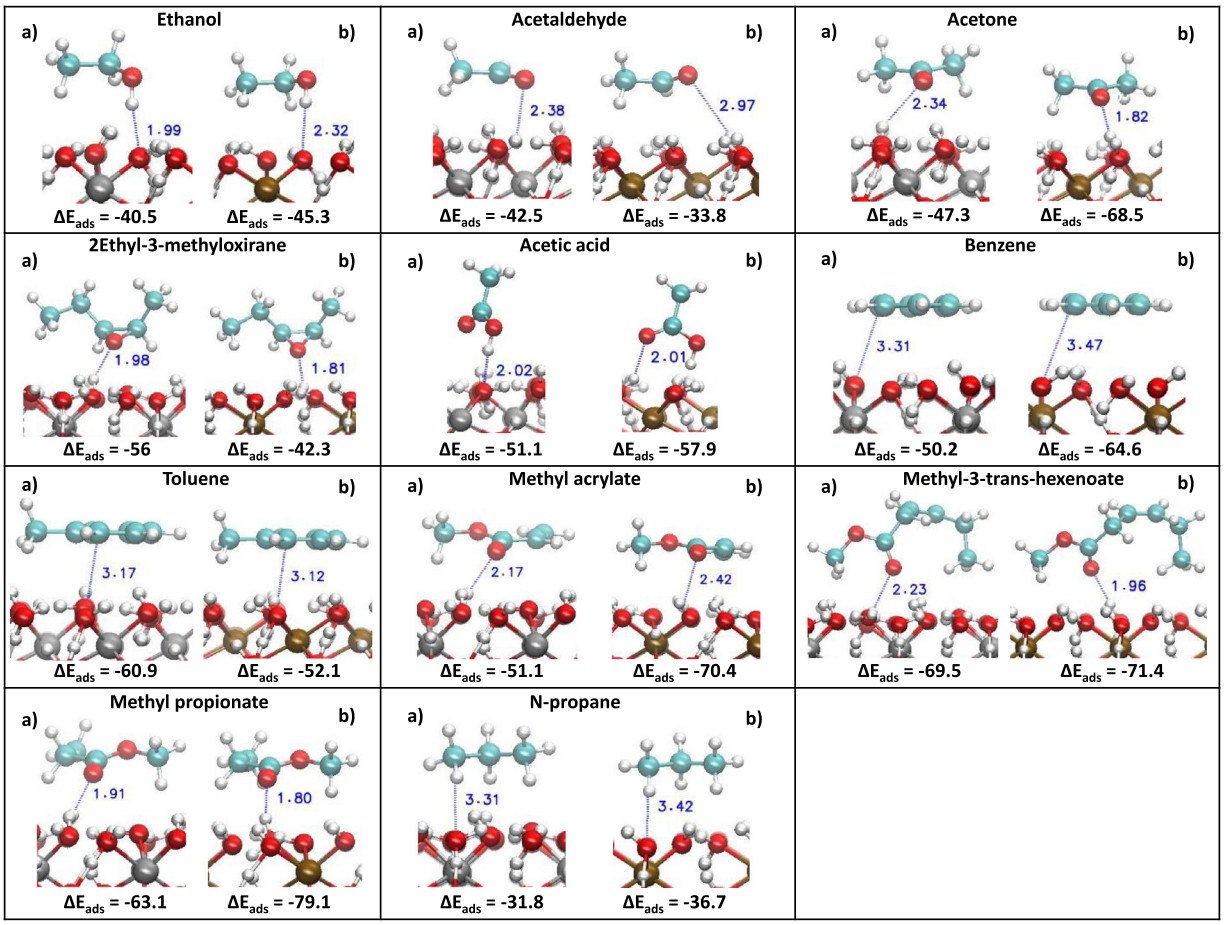

Fig. 6. Optimized adsorption configurations on hydroxylated surfaces with their corresponding adsorption energies calculated via DFT approach of different model molecules on fully-hydroxylated α-Al_2O_3 (a) and α-Cr_2O_3 (b) surfaces respectively. The bond distances are reported in Angstrom [Å] and the adsorption energies in [kJ mol^{-1}]. Color code: red = O; light-blue = C; white: H; gray = Al; brown = Cr.. (For interpretation of the references to color in this figure legend, the reader is referred to the web version of this article.)

coordinate with a polar oxygen atom (or group) to the surface. Such polar groups are missing in benzene and toluene, where the attenuation effect due to the hydration layer is almost absent.

Fig. 7b compares the adsorption energies on hydroxylated Cr_2O_3 and Al_2O_3. The average value is very near the $y = x$ function, suggesting that it is principally the hydration layer that now determines the adsorption energy, and the underlying oxide only plays a secondary role. The charge transfers between the surface and the adsorbed molecules have been calculated and are found to be negligible, ranging between −0.03 and +0.02 electrons.

Finally, regarding the weak interactions, we have analyzed the contribution resulting from the dispersion energy to the total adsorption energy (Fig. 7c). It appears that the weak interactions increase with the molecule size. Also, small differences are seen with the nature of the surface: the van der Waals forces are generally slightly more intense on dry Al_2O_3, with respect to the three other surfaces.

3.3. Temperature desorption of the different molecules

We also considered the free energies of the molecules in the gas phase and deduced the desorption temperature from the surface which results are reported in Table 3 (see calculation details on Section 2.1.1). The gas phase molecular thermochemical data are reported in SI section, Table S3.

Fig. 8 reports the desorption temperature from the hydroxylated surface with respect to the anhydrous one. The left-upper zone corresponds to molecules that have more affinity for the hydroxylated than the anhydrous surface. The right lower zone corresponds to molecules that have more affinity with the anhydrous surface than with the hydroxylated one, and the zone near $y = x$ to molecules that have equivalent affinity with the dry and hydroxylated surfaces. On Al_2O_3 molecules (especially oxygenated molecules) stick predominantly on the anhydrous Al_2O_3 surface until elevated temperatures (500–600 K), whereas most molecules are expected to detach from the Cr_2O_3 surface at temperature above RT, independently on the surface state (hydroxylated versus anhydrous).

The present results suggest that at temperatures of the injection system, around 500 K, the stainless steel surface should be free of residual molecules, but the aluminum surface could be contaminated with water and some oxygenated molecules. Obviously in the operating conditions, the chemical potentials of the diverse species have also to be considered in the thermochemistry evaluations and some species could be further stabilized at the surface.

It is interesting to compare the adsorption of the different molecules with that of water. We calculate water desorption temperatures around 680 K for Al_2O_3 and 450 K for Cr_2O_3. This allows us to identify the molecules susceptible to substitute water at the surface. The results suggest that only acetic acid, which desorption temperature is as high as water, is susceptible to compete with water adsorption on chromia.

3.4. Water/OH substitution

Now we will study explicitly acid acetic that has a marked affinity with the anhydrous surfaces, to which extent water molecule can be exchanged. The results are compared with that on methyl propionate, which, according to our first estimation, is not expected to substitute

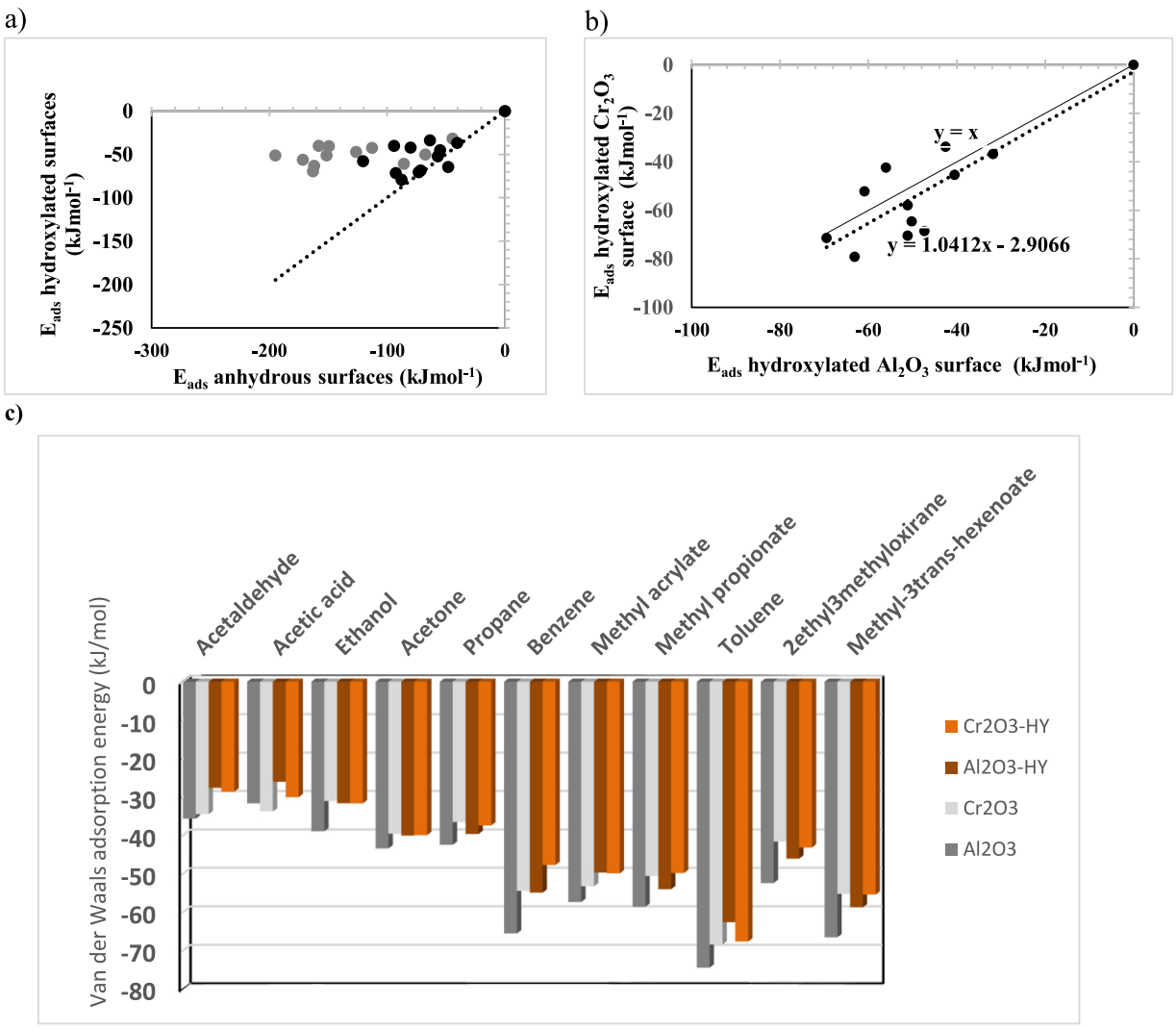

Fig. 7. (a) Adsorption energies (kJ mol $^{-1}$) on the hydroxylated surfaces versus the anhydrous surfaces, black: Cr, gray: Al; (b) Adsorption energies (kJ mol $^{-1}$) on hydroxylated Cr_2O_3 versus hydroxylated Al_2O_3. The linear average curve is plotted in black, dotted line. The identity function ($y = x$) is plotted in black (plain line); c) Contribution of the van der Waals energy to the total adsorption energy of the different molecules on dry Al_2O_3 and Cr_2O_3, and hydroxylated Al_2O_3 and Cr_2O_3. (For interpretation of the references to color in this figure legend, the reader is referred to the web version of this article.)

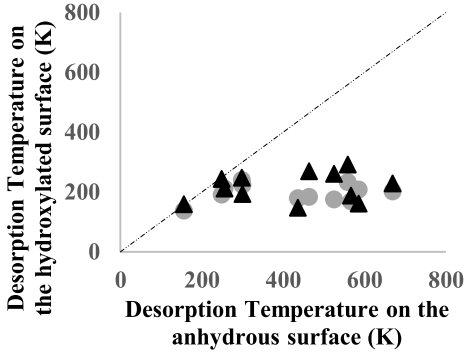

Fig. 8. Desorption temperature on hydroxylated surfaces with respect to the anhydrous surfaces. The $y = x$ line is plotted for a guide to the eye. Black : Cr_2O_3, gray: Al_2O_3.

Table 3
Desorption temperature (K) calculated for the different molecules adsorbed on the M_2O_3, dry and hydroxylated.

Molecule	Tdesorb Al_2O_3 (K)	Tdesorb Al_2O_3-HY (K)	Tdesorb Cr_2O_3 (K)	Tdesorb Cr_2O_3-HY (K)
propane	156	137	179	159
benzene	249	192	188	244
toluene	300	223	211	193
water	678	211	452	211
acetaldehyde	436	179	256	147
acetone	464	184	270	269
methylacrylate	525	175	262	261
hexenoate	298	240	307	247
methylpropionate	559	233	307	291
ethanol	567	168	225	188
oxirane	586	209	282	162
acetic-acid	669	202	443	228

water. In Fig. 9a–b are reported the optimized configurations of the dissociative adsorptions of the acetic acid molecules on fully-hydroxylated α-Cr_2O_3-$Cr(OH)_3$ and α-Al_2O_3-$Al(OH)_3$. The substitution reaction of an OH group by an acetate anion is described by Eq. (2) and consists of an acid–base mechanism with formation of a Cr-molecule adduct and the release of a water molecule in the gas phase. The substitution energy is −43.8 kJ mol^{-1} for chromia, and −17.5 kJ mol^{-1} for Al_2O_3. The

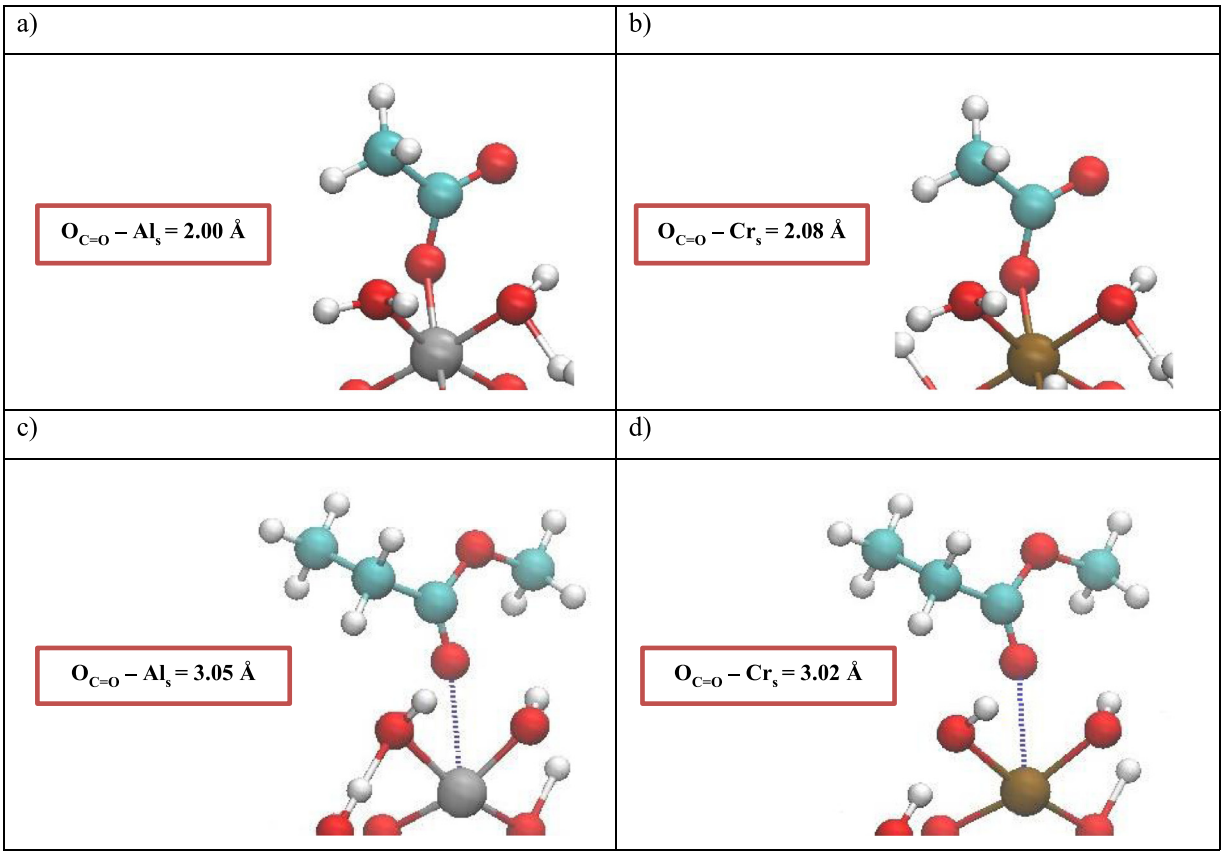

Fig. 9. (a–b) Optimized adsorption configurations calculated via DFT approach of a substitution reaction between an acetic acid and a water molecule on fully hydroxylated α-Al_2O_3-$Al(OH)_3$ (a) and α-Cr_2O_3-$Cr(OH)_3$ (b) respectively. The background atoms of both configurations have been removed for clarity. Color code: Red = O; light-blue = C; white = H; Brown= Cr; Gray = Al.
(c–d): Optimized adsorption configurations calculated via DFT approach of a substitution reaction between a methylpropionate molecule and a water molecule on fully hydroxylated α-Al_2O_3-$Al(OH)_3$ (a) and α-Cr_2O_3-$Cr(OH)_3$ (b) respectively. The background atoms of both configurations have been removed for clarity. Color code: Red = O; light-blue = C; white = H; Brown = Cr; Gray = Al.

substitution of OH by acetate is thus an exothermic process for both surfaces, a trend in agreement with the conclusions of the preceding paragraph.

The results of the substitution reaction of water by methyl propionate are shown in Fig. 9c–d. It can easily be observed that methyl propionate does not get very close to the surfaces. Starting with the Cr-O and Al-O bond lengths obtained on the anhydrous surfaces, 1.88 Å for Al_2O_3 and 2.22 Å for Cr_2O_3 (Fig. 2), we observe that the M-O distances increase on the hydroxylated surfaces to 3.05 Å (Fig. 9c) and 3.02 Å (Fig. 9d), respectively. Complementary calculations of adsorption on partially hydroxylated surfaces were performed in the case of methyl propionate. We found that methyl propionate forms a bond with surface Al only in the totally dehydrated case, but not on the Al-OH and Al-$(OH)_2$ terminations, confirming that methyl propionate binds a bond with Al_{4c} (four fold coordinated) only. The substitution energies are −34.7 and 17 kJ mol^{-1} for Cr_2O_3 and Al_2O_3, respectively. The water substitution by methyl propionate is endothermic for Al_2O_3, as expected from the preceding paragraph, while slightly exothermic on Cr_2O_3.

We can analyze further these results in calculating the different components of the substitution energy: water desorption energy and molecule/surface binding energy, and Table 4 summarizes the values obtained for energy decomposition for MP and acetic acid.

We observe that the substitutive adsorption of methyl propionate and acetic acid are favored on Cr_2O_3 over Al_2O_3. This can be explained by the decomposition of the energy: firstly, water desorption is less endothermic for Cr_2O_3 than Al_2O_3; secondly, the binding energy of MP is slightly more important for Cr_2O_3; thirdly, the relaxation energies are practically equivalent for both surfaces.

We note in the case of acetate adsorption, both a strong molecule–surface interaction and a strong component of the relaxation energy to accommodate the adsorbed anion.

4. Conclusion

To improve our understanding of undesired deposit formations observed for biodiesels in engine fuel circuits, we have conducted a quantum mechanical study using density functional theory calculations on the adsorption of small representative organic molecules on representative aluminum and stainless steel surfaces. The investigated organic compounds comprise hydrocarbons like n-alkanes and aromatic molecules, as well as oxygen containing molecules including an alcohol, aldehyde, ketone, epoxide, carboxylic acid, and esters. The stainless-steel fuel circuit was represented by α-Cr_2O_3 and aluminum-based circuits by α-Al_2O_3, in which each studied surface orientation was either anhydrous or fully hydroxylated.

From this study we determined that:

1. Anhydrous surfaces are more reactive towards the organic molecules than their fully hydroxylated counterparts as seen from the more negative adsorption energies.
2. Aluminum anhydrous surfaces show a higher reactivity as compared to anhydrous chromia, while this difference vanishes upon fully hydroxylating the surfaces.
3. Oxygen containing organic compounds show more negative adsorption energies independent of the nature of the inorganic surface.

Table 4
Energy decomposition for water/OH substitution by methyl propionate/acetate on hydroxylated Al_2O_3 and Cr_2O_3 (kJ mol^{-1})

System	Water desorption (kJ mol^{-1}) Eq. (6)	Binding energy molecule/surface (kJ mol^{-1}) Eq. (7)	Erelax (kJ mol^{-1}) Eq. (8)	Substitution energy (kJ mol^{-1}) Eq. (5)	$\Delta E(Al_2O_3\text{-}Cr_2O_3)$ (kJ mol^{-1})
Methyl propionate@Al_2O_3-HY	54.6	−46.6	9.0	17	51.7
Methyl propionate@Cr_2O_3-HY	22.6	−62.6	5.4	−34.7	
Acetic acid@ Al_2O_3-HY	54.6	−285.1	213	−17.5	26.3
Acetic acid@ Cr_2O_3-HY	22.6	−307.18	240.8	−43.8	

4. Except for the dissociative adsorption of acetic acid on anhydrous α-Al_2O_3 no other significant geometrical changes, e.g. bond elongations, in the organic molecules were observed due to adsorption on the oxide surfaces.
5. Bader charge analyses show that there are only weak charge transfers between the different oxides and organic molecules, expect for the dissociative adsorption of acetic acid on dry alumina.

Since under operational conditions each of the oxide surfaces is at least partially or fully hydroxylated, the difference in nature of the oxides vanishes with respect to its reactivity towards the investigated organic compounds. In other words, based on this study, stainless-steel circuits which is the surface that is more problematic since it is material of injectors, would not play a more important role in the autoxidation reactions as compared to aluminum-based materials. This finding is important since it corroborates that fuel oxidation products aggregates seems to be mainly formed in the liquid phase further being deposited on a surface by different mechanisms (Alves-Fortunato et al., 2020). Furthermore, the relatively weak interactions (–30 to –70 kJ mol^{-1}) between surface and molecule seem to be insufficient to provoke significant distortions in the organic molecule itself, which in turn could lead to higher reactivity and rendering the molecule more prone to autoxidation reactions in liquid phase.

In autoxidation reactions the temperature plays a key role. Yet, in our models, temperature has only been considered indirectly and implicitly. Future works will improve this using molecular dynamics with an empirical reactive force field.

Declaration of competing interest

The authors declare that they have no known competing financial interests or personal relationships that could have appeared to influence the work reported in this paper.

Acknowledgments

This research was carried out in the frame of a doctoral research project financed by IFP Energies nouvelles Scientific Division and supported by IFPEN Transports Energy Carnot Institute. The authors thank the Laboratoire de Physico-Chimie des Surfaces, UMR CNRS-ENSCP 7045, to all extremely valuable support for VASP calculations. Dr. C. Chizallet (IFPEN) is greatly acknowledged for providing alumina model structures and useful discussions. The authors thank GENCI for high performance calculations in the national (CINES) center under the A0040802217.

Appendix A. Supplementary data

Supplementary material related to this article can be found online at https://doi.org/10.1016/j.rsurfi.2022.100050.

Table S1: Calculated (VASP) versus experimental bulk structural parameters of α-Al_2O_3 and Cr_2O_3.

Table S2: Energy, ZPE contribution, Free energy and Entropy contributions of the gaz-phase molecules

Table S3: Intramolecular bonds presenting the highest distortion after adsorption of each molecule on dry α-(0001) Al_2O_3

Fig. S1: Slabs retained for the (0001) surfaces: a–c)4 × 4 cell; d–f):2 × 2 cell.

Fig. S2: Nomenclature for adsorption and dissociation of protic molecules at corundum Al_2O_3 and Cr_2O_3 (0001) surfaces. Top-view of Al_2O_3 or Cr_2O_3 with a metal cation (gray) in the center of 3 oxygen atoms (blue). If the metal (Cr/Al) ion is considered at position 1, the blue (oxygen) atoms are at position 2, and the green (oxygen) at position 4.

References

Alexander, M.R., Beamson, G., Blomfield, C.J., Leggett, G., Duc, T.M., 2001. Interaction of carboxylic acids with the oxyhydroxide surface of aluminium poly(acrylic acid), acetic acid and propionic acid on pseudoboehmite. J. Electron. Spect. Relat. Phenomena 121, 19–32. http://dx.doi.org/10.1016/S0368-2048(01)00324-3.

Alves-Fortunato, M., Ayoub, E., Bacha, K., Mouret, A., Dalmazzone, C., 2020. Fatty acids methyl esters (FAME) autoxidation: New insights on insoluble deposit formation process in biofuels. Fuel 268, 117074. http://dx.doi.org/10.1016/j.fuel.2020.117074.

Alves-Fortunato, M., Labaume, J., Cologon, P., Barré, L., 2018. Biofuel surrogate oxidation: Insoluble deposits formation studied by small-angle X-ray scattering and small angle neutron scattering. Energy Fuels 32, 9559–9567. http://dx.doi.org/10.1021/acs.energyfuels.8b02055.

Alves Fortunato, M., Lenglet, F., Ben Amara, A., Starck, L., 2019. Are internal diesel injector deposits (IDID) mainly linked to biofuel chemical composition or/and engine operation condition? SAE Int. J. Fuels Lubr. http://dx.doi.org/10.4271/2019-01-0061.

Anisimov, V.I., Aryasetiawan, F., Lichtenstein, A.I., 1997. First-principles calculations of the electronic structure and spectra of strongly correlated systems: the LDA + U method. J. Phys.: Condens. Matter 9, 767–808. http://dx.doi.org/10.1088/0953-8984/9/4/002.

Arrouvel, C., Breysse, M., Toulhoat, H., Raybaud, P., 2005. A density functional theory comparison of anatase (TiO2)- and γ-Al2O3-supported MoS2 catalysts. J. Catal. 232, 161–178. http://dx.doi.org/10.1016/j.jcat.2005.02.018.

Arrouvel, C., Diawara, B., Costa, D., Marcus, P., 2007. DFT periodic study of the adsorption of glycine on the anhydrous and hydroxylated (0001) surfaces of α-alumina. J. Phys. Chem. C 111, 18164–18173. http://dx.doi.org/10.1021/jp0741408.

Arrouvel, C., Digne, M., Breysse, M., Toulhoat, H., Raybaud, P., 2004a. Effects of morphology on surface hydroxyl concentration: a DFT comparison of anatase–TiO2 and γ-alumina catalytic supports. J. Catal. 222, 152–166. http://dx.doi.org/10.1016/j.jcat.2003.10.016.

Arrouvel, C., Toulhoat, H., Breysse, M., Raybaud, P., 2004b. Effects of PH2O, PH2S, PH2 on the surface properties of anatase -TiO2 and γ-Al2O3: a DFT study. J. Catal. 226, 260–272. http://dx.doi.org/10.1016/j.jcat.2004.05.019.

Bacha, K., 2016. These de Doctorat Etude de l'interaction entre le carburant diesel et les composants su systèmes d'injection diesel. Phys. Des Matériaux.

Bacha, K., Ben-Amara, A., Vannier, A., Alves-Fortunato, M., Nardin, M., 2015. Oxidation stability of diesel/biodiesel fuels measured by a PetroOxy device and characterization of oxidation products. Energy Fuels 29, 4345–4355. http://dx.doi.org/10.1021/acs.energyfuels.5b00450.

Bahlakeh, G., Ghaffari, M., Saeb, M.R., Ramezanzadeh, B., de Proft, F., Terryn, H., 2016. A close-up of the effect of iron oxide type on the interfacial interaction between epoxy and carbon steel: Combined molecular dynamics simulations and quantum mechanics. J. Phys. Chem. C 120, 11014–11026. http://dx.doi.org/10.1021/acs.jpcc.6b03133.

Baran, J.D., Grönbeck, H., Hellman, A., 2014. Mechanism for limiting thickness of thin oxide films on aluminum. Phys. Rev. Lett. 112, 146103–1–146103–5. http://dx.doi.org/10.1103/PhysRevLett.112.146103-146103-5.

Barker, J., Reid, J., Snape, C., Scurr, D., Meredith, W., 2014. Spectroscopic studies of internal injector deposits (IDID) resulting from the use of non-commercial low molecular weight polyisobutylenesuccinimide (PIBSI). SAE Int. J. Fuels Lubr. 7, 762–770. http://dx.doi.org/10.4271/2014-01-2720.

Bender, M., et al., 1995. Structural rearrangement and surface magnetism on oxide surfaces a temperature-dependent low-energy electron diffraction-electron energy loss spectroscopy study of Cr2O3(111)/Cr(110). J. Phys.: Condens. Matter 7, 5289–5302. http://dx.doi.org/10.1088/0953-8984/7/27/014.

Bikondoa, O., Moritz, W., Torrelles, X., Kim, H.J., Thornton, G., Lindsay, R., 2010. Impact of ambient oxygen on the surface structure of α-Cr2O3(0001). Phys. Rev. B 81, http://dx.doi.org/10.1103/PhysRevB.81.205439.

Blanck, S., Loehlé, S., Steinmann, S.N., Michel, C., 2020. Adhesion of lubricant on aluminium through adsorption of additive head-groups on γ-alumina: A DFT study. Tribol. Int. 145, 106140. http://dx.doi.org/10.1016/j.triboint.2019.106140.

Blanck, S., Martí, C., Loehlé, S., Steinmann, S.N., Michel, C., 2021. (Dis) similarities of adsorption of diverse functional groups over alumina and hematite depending on the surface state. J. Chem. Phys. 154, 84701. http://dx.doi.org/10.1063/5.0038412.

Borck, Ø., Hyldgaard, P., Schröder, E., 2007. Adsorption of methylamine on α-Al2O3(0001) and α-Cr2O3(0001) Density functional theory. Phys. Rev. B 75, http://dx.doi.org/10.1103/PhysRevB.75.035403.

Borck, Ø., Schröder, E., 2006a. First-principles study of the adsorption of methanol at the α-Al 2O3 (0001) surface. J. Phys.: Condens. Matter 18, 1–12. http://dx.doi.org/10.1088/0953-8984/18/1/001.

Borck, Ø., Schröder, E., 2006b. First-principles study of the adsorption of methanol at the α-Al2O3 (0001) surface. J. Phys.: Condens. Matter 18, 1–12. http://dx.doi.org/10.1088/0953-8984/18/1/001.

Botella, R., Chiter, F., Costa, D., Nakashima, S., Lefèvre, G., 2021. Influence of hydration/dehydration on adsorbed molecules: Case of phthalate on goethite. Colloids Surf. A Physicochem. Eng. Asp. 625, 126872. http://dx.doi.org/10.1016/j.colsurfa.2021.126872.

Chakarova-Käck, S.D., Borck, Ø., Schröder, E., Lundqvist, B.I., 2006. Adsorption of phenol on graphite(0001) and α-Al2O3(0001) Nature of van der Waals bonds from first-principles calculations. Phys. Rev. B 74, http://dx.doi.org/10.1103/PhysRevB.74.155402.

Chatelain, K., Nicolle, A., Ben Amara, A., Catoire, L., Starck, L., 2016. Wide range experimental and kinetic modeling study of chain length impact on n -alkanes autoxidation. Energy Fuels 30, 1294–1303. http://dx.doi.org/10.1021/acs.energyfuels.5b02470.

Corporan, E., Edwards, T., Shafer, L., DeWitt, M.J., Klingshirn, C., Zabarnick, S., West, Z., Striebich, R., Graham, J., Klein, J., 2011. Chemical, thermal stability, seal swell, and emissions studies of alternative jet fuels. Energy Fuels 25, 955–966. http://dx.doi.org/10.1021/ef101520v.

Costa, D., Ribeiro, T., Mercuri, F., Pacchioni, G., Marcus, P., 2014. Atomistic modeling of corrosion resistance: A first principles study of O2 reduction on the Al(111) surface covered with a thin hydroxylated alumina film. Adv. Mater. Interfaces 1, 1300072. http://dx.doi.org/10.1002/admi.201300072.

Costa, D., Sharkas, K., Islam, M.M., Marcus, P., 2009. Ab initio study of the chemical states of water on Cr2O3(0001): From the isolated molecule to saturation coverage. Surf. Sci. 603, 2484–2493. http://dx.doi.org/10.1016/j.susc.2009.05.037.

Dabaghmanesh, S., Neyts, E.C., Partoens, B., 2016. Van der waals density functionals applied to corundum-type sesquioxides: Bulk properties and adsorption of CH3 and C6H6 on (0001) surfaces. Phys. Chem. Chem. Phys. 18, 23139–23146. http://dx.doi.org/10.1039/c6cp00346.

Di Felice, R., Northrup, J.E., 1999. Theory of the clean and hydrogenated Al2O3 (0001) - (1x1) surfaces. Phys. Rev. B 60, 16287–16290. http://dx.doi.org/10.1103/PhysRevB.60.R16287.

Digne, M., Sautet, P., Raybaud, P., Euzen, P., Toulhoat, H., 2002. Hydroxyl groups on γ-alumina surfaces: A DFT study. J. Catal. 211, 1–5. http://dx.doi.org/10.1006/jcat.2002.3741.

Frisch, M.J., Trucks, G.W., Schlegel, H.B., Scuseria, G.E., Robb, M.A., Cheeseman, J.R., Scalmani, G., Barone, V., Petersson, G.A., Nakatsuji, H., Li, X., Caricato, M., Marenich, A.V., Bloino, J., Janesko, B.G., Gomperts, R., Mennucci, B., Hratchian, H.P., Ortiz, J.V., Izmaylov, A.F., Sonnenberg, J.L., Williams, Ding, F., Lipparini, F., Egidi, F., Goings, J., Peng, B., Petrone, A., Henderson, T., Ranasinghe, D., Zakrzewski, V.G., Gao, J., Rega, N., Zheng, G., Liang, W., Hada, M., Ehara, M., Toyota, K., Fukuda, R., Hasegawa, J., Ishida, M., Nakajima, T., Honda, Y., Kitao, O., Nakai, H., Vreven, T., Throssell, K., Jr, J.A. Montgomery, Peralta, J.E., Ogliaro, F., Bearpark, M.J., Heyd, J.J., Brothers, E.N., Kudin, K.N., Staroverov, V.N., Keith, R., Kobayashi, J., Normand, K., Raghavachari, A.P., Rendell, J.C., Burant, S.S., Iyengar, J., Tomasi, M., Cossi, J.M., Millam, M., Klene, C., Adamo, R., Cammi, J.W., Ochterski, R.L., Martin, K., Morokuma, O., Farkas, J.B., Foresman, D.J., Fox, T.A., 2016. Gaussian 16 Rev. C.01. Gaussian. Inc. Wallingford, E.U.A..

Gouron, A., Kittel, J., de Bruin, T., Diawara, B., 2015. Density functional theory study of monoethanolamine adsorption on hydroxylated Cr2O3 surfaces. J. Phys. Chem. C 119, 22889–22898. http://dx.doi.org/10.1021/acs.jpcc.5b05375.

Grimme, S., Antony, J., Ehrlich, S., Krieg, H., 2010. A consistent and accurate ab initio parametrization of density functional dispersion correction (DFT-D) for the 94 elements H-Pu. J. Chem. Phys. 132, 154104. http://dx.doi.org/10.1063/1.3382344.

Grinstead, B., Zabarnick, S., 1999. Studies of jet fuel thermal stability, oxidation, and additives using an isothermal oxidation apparatus equipped with an oxygen sensor. Energy Fuels 13, 756–760.

Hafidi, A., Anglaret, E., Pioch, D., Ajana, H., 2004. Characterization of vegetable oils-alumina membranes interactions by diffuse reflectance Fourier transform infrared spectroscopy. Eur. J. Lipid Sci. Technol. 106, 11–21. http://dx.doi.org/10.1002/ejlt.200300851.

Hass, K.C., Schneider, W.F., Curioni, A., Andreoni, W., 1998. The chemistry of water on alumina surfaces: reaction dynamics from first principles. Science 282, 265–268. http://dx.doi.org/10.1126/science.282.5387.265.

Hass, K.C., Schneider, W.F., Curioni, A., Andreoni, W., 2000. First-principles molecular dynamics simulations of H2O on α-Al2O3 (0001). J. Phys. Chem. B 104, 5527–5540. http://dx.doi.org/10.1021/jp000040p.

Heiden, S., Usvyat, D., Saalfrank, P., 2019. Theoretical surface science beyond gradient-corrected density functional theory: Water at α-Al2O3 (0001) as a Case Study. J. Phys. Chem. C 123, 6675–6684. http://dx.doi.org/10.1021/acs.jpcc.9b00407.

Hsissou, R., 2021. Review on epoxy polymers and its composites as a potential anticorrosive coatings for carbon steel in 3.5% NaCl solution: Computational approaches. J. Mol. Liq. 336, 116307. http://dx.doi.org/10.1016/j.molliq.2021.116307.

Hsissou, R., Abbout, S., Benhiba, F., Seghiri, R., Safi, Z., Kaya, S., Briche, S., Serdaroğlu, G., Erramli, H., Elbachiri, A., Zarrouk, A., El Harfi, A., 2021. Insight into the corrosion inhibition of novel macromolecular epoxy resin as highly efficient inhibitor for carbon steel in acidic mediums: Synthesis, characterization, electrochemical techniques, AFM/UV–Visible and computational investigations. J. Mol. Liq. 337, 116492. http://dx.doi.org/10.1016/j.molliq.2021.116492.

Hsissou, R., Abbout, S., Seghiri, R., Rehioui, M., Berisha, A., Erramli, H., Assouag, M., Elharfi, A., 2020a. Evaluation of corrosion inhibition performance of phosphorus polymer for carbon steel in [1 M] HCl: Computational studies (DFT, MC and MD simulations). J. Mater. Res. Technol. 9, 2691–2703. http://dx.doi.org/10.1016/j.jmrt.2020.01.002.

Hsissou, R., Benhiba, F., Abbout, S., Dagdag, O., Benkhaya, S., Berisha, A., Erramli, H., Elharfi, A., 2020b. Trifunctional epoxy polymer as corrosion inhibition material for carbon steel in 1.0 M HCl: MD simulations, DFT and complexation computations. Inorg. Chem. Commun. 115, 107858. http://dx.doi.org/10.1016/j.inoche.2020.107858.

Huš, M., Kopač, D., Likozar, B., 2020. Kinetics of non-oxidative propane dehydrogenation on cr2o3 and the nature of catalyst deactivation from first-principles simulations. J. Catal. 386, 126–138. http://dx.doi.org/10.1016/j.jcat.2020.03.037.

Jenness, G.R., Christiansen, M.A., Caratzoulas, S., Vlachos, D.G., Gorte, R.J., 2014. Site-dependent lewis acidity of γ-Al2O3 and its impact on ethanol dehydration and etherification. J. Phys. Chem. C 118, 12899–12907. http://dx.doi.org/10.1021/jp5028349.

Kistamurthy, D., Saib, A.M., Moodley, D.J., Preston, H., Ciobîcă, I.M., van Rensburg, W.J., Niemantsverdriet, J.W., Weststrate, C.J., 2016. The role of carboxylic acid in cobalt Fischer–Tropsch synthesis catalyst deactivation. Catal. Today 275, 127–134. http://dx.doi.org/10.1016/j.cattod.2015.11.012.

Kresse, Hafner, 1993. Ab initio molecular dynamics for liquid metals. Phys. Rev. B 47, 558–561. http://dx.doi.org/10.1103/PhysRevB.47.558.

Kresse, G., Furthmuller, J., 1996. Efficiency of ab-initio total energy calculations for metals and semiconductors using a plane-wave basis set. Comput. Mater. Sci. 6, 15–50. http://dx.doi.org/10.1016/0927-0256(96)00008-0.

Kresse, G., Furthmüller, J., 1996. Efficient iterative schemes for ab initio total-energy calculations using a plane-wave basis set. Phys. Rev. B 54, 11169–11186. http://dx.doi.org/10.1103/physrevb.54.11169.

Kresse, G., Hafner, J., 1994. Ab initio molecular-dynamics simulation of the liquid-metal-amorphous-semiconductor transition in germanium. Phys. Rev. B 49, 12252–14269. http://dx.doi.org/10.1103/PhysRevB.49.14251.

Kumar, A., Ropital, F., de Bruin, T., Diawara, B., 2020. Effects of surface orientations of Cr2O3 on CO2 adsorption: A DFT approach. Appl. Surf. Sci. 529, 147127. http://dx.doi.org/10.1016/j.apsusc.2020.147127.

Lacey, P., Gail, S., Kientz, J.M., Benoist, G., Downes, P., Daveau, C., 2012. Fuel quality and diesel injector deposits. SAE Int. J. Fuels Lubr. 5, 1187–1198. http://dx.doi.org/10.4271/2012-01-1693.

Li, X., Wang, S., Zhu, Y., Yang, G., Zheng, P., 2015. DFT study of bio-oil decomposition mechanism on a Co stepped surface: Acetic acid as a model compound. Int. J. Hydrog. Energy 40, 330–339. http://dx.doi.org/10.1016/j.ijhydene.2014.11.004.

Lim, M.S., Feng, K., Chen, X., Wu, N., Raman, A., Nightingale, J., Gawalt, E.S., Korakakis, D., Hornak, L.A., Timperman, A.T., 2007. Adsorption and desorption of stearic acid self-assembled monolayers on aluminum oxide. Langmuir 23, 2444–2452. http://dx.doi.org/10.1021/la061914n.

Łodziana, Z., Nørskov, J.K., Stoltze, P., 2003. The stability of the hydroxylated (0001) surface of α-Al2O3. J. Chem. Phys. 118, 11179–11188. http://dx.doi.org/10.1063/1.1574798.

Lübbe, M., Moritz, W., 2009. A LEED analysis of the clean surfaces of α-Fe(2)O(3)(0001) and α-Cr(2)O(3)(0001) bulk single crystals. J. Phys.: Condens. Matter 21, http://dx.doi.org/10.1088/0953-8984/21/13/134010.

Massoud, T., Maurice, V., Klein, L.H., Seyeux, A., Marcus, P., 2014. Nanostructure and local properties of oxide layers grown on stainless steel in simulated pressurized water reactor environment. Corros. Sci. 84, 198–203. http://dx.doi.org/10.1016/j.corsci.2014.03.030.

Matthew, J., Lane, D., Leung, K., Thompson, A.P., Cuneo, M.E., 2018. Water desorption from rapidly-heated metal oxide surfaces - first principles molecular dynamics and the temkin isotherm. J. Phys.: Condens. Matter 30, 1–32. http://dx.doi.org/10.1088/1361-648X/aae4af.

Mei, D., Dai, S., Chen, T., Wang, H., Yuan, Y., 2020. Absorption of fuel containing esters on iron surface based on molecular simulation and its effects on lubricity. Energ. Sources, Part A 1–12. http://dx.doi.org/10.1080/15567036.2020.1783395.

Monkhorst, H.J., Pack, J.D., 1976. Special points for Brouillon-zone integrations. Phys. Rev. B 13, 5188–5192. http://dx.doi.org/10.1103/PhysRevB.13.5188.

Nigussa, K.N., Nielsen, K.L., Borck, Ø., Støvneng, J.A., 2011. Adsorption of hydrogen, chlorine, and sulfur atoms on α-Cr2O3(0001) surfaces: A density functional theory investigation. Corros. Sci. 53, 3612–3622. http://dx.doi.org/10.1016/j.corsci.2011.07.005.

Pan, Y., Liu, C., Ge, Q., 2008. Adsorption and protonation of CO2 on partially hydroxylated gamma-Al2O3 surfaces: a density functional theory study. Langmuir 24, 12410–12419. http://dx.doi.org/10.1021/la802295x.

Pan, Y., Liu, C., Ge, Q., 2010. Effect of surface hydroxyls on selective CO2 hydrogenation over Ni4/γ-Al2O3: A density functional theory study. J. Catal. 272, 227–234. http://dx.doi.org/10.1016/j.jcat.2010.04.003.

Perdew, John P., Burke, K., Ernzerhof, M., 1996. Generalized gradient approximation made simple. Phys. Rev. Lett. 77, 3865–3868. http://dx.doi.org/10.1103/PhysRevLett.77.3865.

Ranea, V.A., Carmichael, I., Schneider, W.F., 2009. DFT investigation of intermediate steps in the hydrolysis of α-Al 2 O 3 (0001). J. Phys. Chem. C 113, 2149–2158. http://dx.doi.org/10.1021/jp8069892.

Renaud, G., 1998. Oxide surface and metal/oxide interfaces studied by grazing incidence X-ray scattering. Surf. Sci. Rep. 32, 1–90.

Richter, B., Crusius, S., Schümann, U., Handorf, H., 2013. Characterisation of internal deposits in common-rail injectors. MTZ Worldwide 74, 50–56.

Rohrbach, A., Hafner, J., Kresse, G., 2004. Ab initio study of the (0001) surfaces of hematite and chromia: Influence of strong electronic correlations. Phys. Rev. B 70, 13. http://dx.doi.org/10.1103/PhysRevB.70.125426.

Rubasinghege, G., Ogden, S., Baltrusaitis, J., Grassian, V.H., 2013. Heterogeneous uptake and adsorption of gas-phase formic acid on oxide and clay particle surfaces: the roles of surface hydroxyl groups and adsorbed water in formic acid adsorption and the impact of formic acid adsorption on water uptake. J. Phys. Chem. A 117, 11316–11327. http://dx.doi.org/10.1021/jp408169w.

Shukla, M.K., Hill, F., 2013. Computational investigation of adsorption of 2, 4, 6-trinitrotoluene on (0001) surface of (4 ×4) α-alumina. J. Phys. Chem. C 117, 13136–13142. http://dx.doi.org/10.1021/jp403499p.

Siegel, D.J., Hector, L.G., Adams, J.B., 2002. Adhesion, atomic structure, and bonding at the Al(111)/α-Al2O3(0001) interface: A first principles study. Phys. Rev. B 65, http://dx.doi.org/10.1103/PhysRevB.65.085415.

Soleymanibrojeni, M., Shi, H., Liu, F., Han, E.-H., 2020. Atomistic simulations of Epoxy/Water/Aluminum systems using the ReaxFF method. Comput. Mater. Sci. 173, 109424. http://dx.doi.org/10.1016/j.commatsci.2019.109424.

Souvi, S.M., Badawi, M., Virot, F., Cristol, S., Cantrel, L., Paul, J.-F., 2017. Influence of water, dihydrogen and dioxygen on the stability of the Cr 2 O 3 surface: A first-principles investigation. Surf. Sci. 666, 44–52. http://dx.doi.org/10.1016/j.susc.2017.08.005.

Tepesch, P.D., Quong, A.A., 2000. First-principles calculations of ?-alumina (0001) surfaces energies with and without hydrogen. Phys. Stat. Sol. (B) 217, 377–387. http://dx.doi.org/10.1002/(SICI)1521-3951(200001)217:1%3C377:AID-PSSB377%3E3.0.CO;2-B.

Ullmann, J., Geduldig, M., Stutzenberger, H., Caprotti, R., Balfour, G., 2008. Investigation into the formation and prevention of internal diesel injector deposits. SAE Int. J. Fuels Lubr. http://dx.doi.org/10.4271/2008-01-0926.

Wang, X.-G., Chaka, A., Scheffler, M., 2000. Effect of the environment on alpha-Al2O3 (0001) surface structures. Phys. Rev. Lett. 84, 3650–3653. http://dx.doi.org/10.1103/PhysRevLett.84.3650.

Wang, Y., Yan, X., Xiao, W., Shao, Y., 2017. DFT analysis of the adsorption of methyl nitrate on Al2O3 surfaces. Bull. Korean Chem. Soc. 38, 625–631. http://dx.doi.org/10.1002/bkcs.11136.

WEO, I., 2017. International Energy Agency. World Energy Outlook: https://www.iea.org/world-energy-outlook-2017.

Wischert, R., Laurent, P., Copéret, C., Delbecq, F., Sautet, P., 2012. γ-Alumina: the essential and unexpected role of water for the structure, stability, and reactivity of defect sites. J. Am. Chem. Soc. 134, 14430–14449. http://dx.doi.org/10.1021/ja3042383.

Wittbrodt, J.M., Hase, W.L., Schlegel, H.B., 1998. Ab initio study of the interaction of water cluster models of the aluminum terminated (0001) α-aluminum oxide surface. J. Phys. Chem. B 102, 6539–6548. http://dx.doi.org/10.1021/jp981516w.

Xu, L., Hu, Y., Dong, F., Gao, Z., Wu, H., Wang, Z., 2014. Anisotropic adsorption of oleate on diaspore and kaolinite crystals: Implications for their flotation separation. Appl. Surf. Sci. 321, 331–338. http://dx.doi.org/10.1016/j.apsusc.2014.10.042.

Zhang, M., Huang, Y., Li, R., Li, G., Yu, Y., 2014. A DFT study of ethanol adsorption and dehydrogenation on Cu/Cr2O3 catalyst. Catal. Lett. 144, 1978–1986. http://dx.doi.org/10.1007/s10562-014-1356-8.